7

Topographical Change of Engineering Surface due to Running-in of Rolling Contacts

R. Ismail[1], M. Tauviqirrahman[1], Jamari[2] and D.J. Schipper[1]
[1]*Laboratory for Surface Technology and Tribology, University of Twente*
[2]*Laboratory for Engineering Design and Tribology, University of Diponegoro*
[1]*The Netherlands*
[2]*Indonesia*

"If condition were wrong, piston rings could disappear within 24 h after start up, whereas after successful run-in piston ring life could be two years." (Summers-Smith, 1997)

1. Introduction

The above quotation indicates the important of running-in phase, which occurs at the beginning of the contact in a mechanical systems. Tribologist identifies that running-in takes place on the first stages of the practical mechanical system operation such as automotive engines, gears, camshaft and followers, and bearings. Kehrwald (1998) expressed the significance of running-in phase by predicting that an optimized running-in procedure has a potency to improve the life time of a mechanical system by 40% and more and to reduce the engine friction without any material modification.

The running-in phase is known as a transient phase where many parameters seek their stabilize form. During running-in, the system adjusts to reach a steady-state condition between contact pressure, surface roughness, interface layer, and the establishment of an effective lubricating film at the interface. These adjustments may cover surface conformity, oxide film formation, material transfer, lubricant reaction product, martensitic phase transformation, and subsurface microstructure reorientation (Hsu, et al., 2005). Next, the running-in phase is followed by a steady state phase which is defined as the condition of a given tribo-system in which the average dynamic coefficient of friction, specific wear rate, and other specific parameters have reached and maintained a relatively constant level (Blau, 1989).

Due to the complexity of the involved parameters, the discussion of running-in in this book chapter will be focused on the topographical change, contact stress and residual stress of an engineering surface which is caused by rolling contact of a smooth body over a rough surface. Specifically, the attention will be concentrated on the asperity of the rough surface. There are many applications of the rolling contact in mechanical components system, such as in bearing components, etc., therefore, the observation of the running-in of rolling contact becomes an interesting subject. The obvious examples are the contact of the thrust roller bearing and deep groove ball bearing where the running-in occurs on the rings. Its initial

topography, friction, and lubrication regime change due to the contact with the balls on the first use of the bearing lifespan history.
This chapter is devided into six sub-chapters which the first sub-chapter deals with the significance of running-in as introduction. It is continued with the definition of "rolling contact" and "running-in" including with the types classification in sub-chapter 2 and 3, respectively. In sub-chapter 4, the model of running-in of rolling contact is studied by presenting an analytical model and numerical simulation using finite element analysis (FEA). A running-in model, derived analytically based on the static contact equation on the basis of ellipsoid deformation model (Jamari & Schipper, 2006) which is applied deterministically (Jamari & Schipper, 2008) on the real engineering surface, is proposed and verified with the experimental investigations. The topographical evolution from the initial to the final surface during running-in of rolling contact is presented. The numerical simulations of the two-dimensional FEA on the running-in of rolling contact are employed for capturing the plastic deformation, the stress and the residual stress. The localized deformations on the summit of the asperities and the transferred materials are discussed as well as the surface and subsurface stresses of the engineering surface during and after repeated rolling contacts. In sub-chapter 5, the experimental investigations, conducted by Jamari (2006) and Tasan et al. (2007), are explored to depics the topographical change of the engineering surface during running-in of rolling contact. With the semi-online measurement system, the topographical change is observed. The longitudinal and lateral change of the surface topography for several materials are presented. The last, concluding remarks close the chapter with some conclusions.

2. Rolling contacts

2.1 Definition of rolling contact

When two non-conformal contacting bodies are pressed together so that they touch in a point or a line contact and they are rotated relatively so that the contact point/line moves over the bodies, there are three possibilities (Kalker, 2000). First, the motion is defined as rolling contact if the velocities of the contacting point/line over the bodies are equal at each point along the tangent plane. Second, it is defined as sliding and the third is rolling with sliding motion.
According to Johnson (1985), a combination between rolling, sliding and spinning can be occured during the rolling of two contacting bodies, either for line contact or point contact. By considering the example of the line contact between body *1* and body *2*, as is shown in the Fig. 1, the rolling contact is defined as the relative angular velocity between the two bodies about an axis lying in the tangent plane. Sliding or slip is indentified as the relative velocity between the two bodies or surfaces at the contact point O in the tangent plane, whereas the spinning is the relative angular velocity between the two bodies about the common normal through O.

2.2 Types of rolling contact

Based on the contact area, the problems of rolling can be divided in three types (Kalker, 2000). (a) Problem in which the contact area is almost flat. The examples are a ball rolling over a plane; an offset printing press; and an automotive wheel rolling over a road. (b) Problems with non-conformal contact in the rolling direction plane and curved in the lateral. The examples are a railway wheel rolling over a rail and a ball rolling in a deep groove, as in ball bearings. (c) Problems in which the contact area is curved in the rolling direction, and conforming in the lateral direction where the example is a pin rolling in a hole.

In the case of rolling friction where the friction takes place on the rolling contact motion and produce the resistance to motion, Halling (1976) classified the rolling contact into: (a) Free rolling, (b) Rolling subjected to traction, (c) Rolling in conforming grooves and (d) Rolling around curves. Whenever rolling occurs, free rolling friction must occur, whereas (b), (c) and (d) occur separately or in combination, depending on the particular situation. The wheel of a car involves (a) and (b), in a radial ball bearing, (a), (b) and (c) are involved, whereas in a thrust ball bearing, (a), (b), (c) and (d) occur.

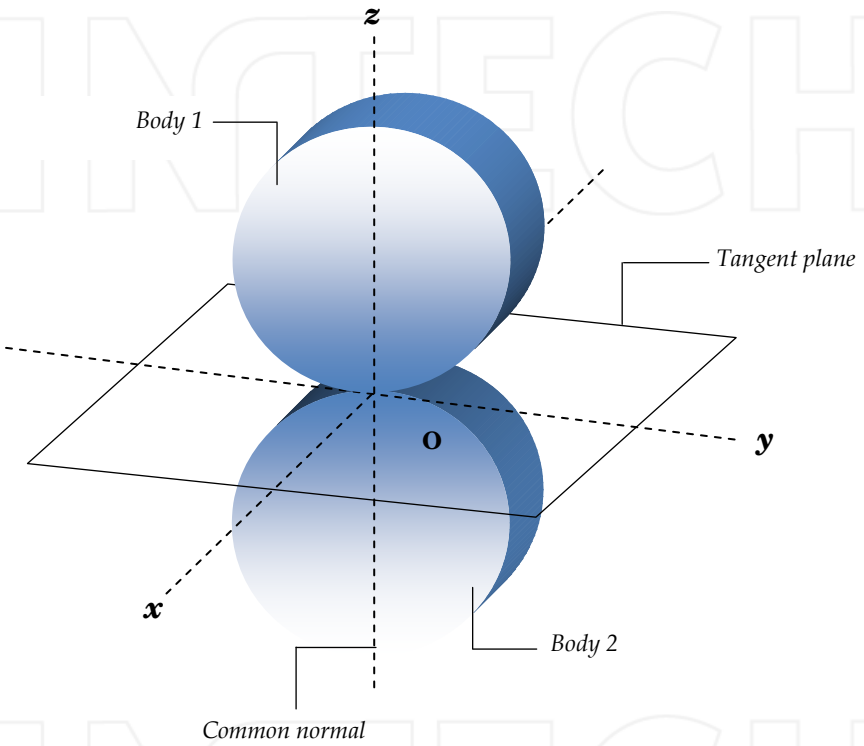

Fig. 1. Line contact between two non-conformal bodies, depicted on the coordinate system

Depending on the forces acting on the contacting bodies, rolling can be classified as free rolling and tractive rolling. Free rolling is used to describe a rolling motion in which there is no slip and the tangential force at the contacting point/line is zero. The term tractive rolling is used when the tangential force in the point/line of contact is not zero or a slip is exist.

3. Running-in

3.1 The definition of running-in

By definition, Summer-Smith (1994) describes running-in as: "The removal of high spots in the contacting surfaces by wear or plastic deformation under controlled conditions of running giving improved conformability and reduced risk of film breakdown during

normal operation". While GOST (former USSR) Standard defines running-in as: "The change in the geometry of the sliding surfaces and in the physicomechanical properties of the surface layers of the material during the initial sliding period, which generally manifests itself, assuming constant external conditions, in a decrease in the frictional work, the temperature, and the wear rate" (Kraghelsky et al., 1982).

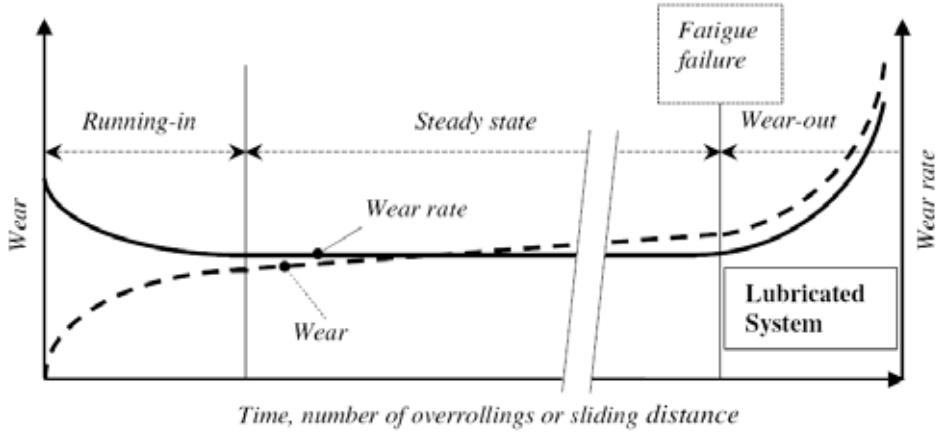

Fig. 2. Schematic representation of the wear behavior as a function of time, number of overrollings or sliding distance of a contact under constant operating conditions (Jamari, 2006)

Generally, the running-in, which is related to the terms breaking-in and wearing-in (Blau, 1989), has been connected to the process by which contacting machine parts improve in conformity, surface topography and frictional compatibility during the initial stage of use. It is focused on the interactions, which take place at the contacted interface on the macro scale and asperity scale, and involves the transition in the existing surface physical condition. For instance in gears contact of the transmission system, the tribologist observes the transition from the unworn to the worn state, from one surface roughness to another surface roughness, from one contact pressure to another contact pressure, from one frictional condition to another, etc. However, the physical change on the contacting surface in this phase, it also can be categorized as "physical damage" at the asperity level, is more beneficial instead of detrimental.

Lin and Cheng (1989) divided three types of wear-time behavior. Majority of the wear time curves observed is of type I, in which the wear rate is initially high and then decrease to a lower value. Wear of type II is more usually observed under dry conditions and the wear rate is constant in time, whilst wear rate of type III is increasing continuously with time. Jamari (2006) presented the wear-time curve which consists of three wear regimes: running-in, the steady state and accelerated wear/wear out as shown in Fig. 2. Each regime has a different wear behavior.

During running-in, the wear-time curve belongs to wear regime of type I. The surface of the material gets adjusted to the contact condition and the operating environment. Wear regime of type II usually takes place in the steady state wear process where the wear-time function is linear. In the wear out regime, the wear rate increases rapidly because of the fatigue wear

which occurs on the upper layers of the loaded surface. The dynamic loading causes fatigue on the surface and results in larger material loss than small fragments associated with adhesive or abrasive wear mechanism. Breakdown of lubrication due to temperature increase, lubricant contaminant or environment factors are other causes of the increase of wear and wear rate in this regime (Lin & Cheng, 1989).

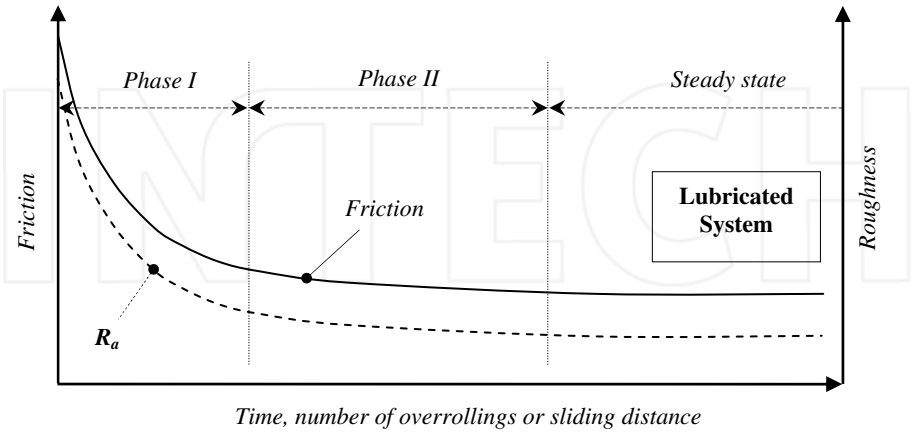

Fig. 3. The change of the coefficient of friction and a roughness as a function of time, number of overrollings or sliding distance of a contact under constant operating conditions (Jamari, 2006)

Figure 3 depicts the friction and roughness decrease as a function of time, the number of overrollings and/or sliding distance. In the running-in phase, the changes of coefficient of friction and roughness in surface topography is required to adjust or minimize energy flow, between moving surface (Whitehouse, 1980). Based on Fig. 3, phase I is indicated by the striking decrease of the surface roughness and the coefficient of friction. On phase II, the micro-hardness and the surface residual stress increases by work hardening and the changes in the geometry of the contact affects the contact behavior in repetitive contacts which leads only a slight decrease of the coefficient of friction and surface roughness. After a steady state condition is obtained, where there is no significant change in coefficient of friction, the full service condition can be applied appropriate with design specifications. The steady state phase is desirable for machine components to operate as long as possible.

3.2 The types of running-in

3.2.1 Based on the shape of the coefficient of friction

Blau (1981) started his work in determining the running-in behavior by collecting numerous examples of running-in experiments and conducting the laboratory experiments which resulted in sliding coefficient of friction versus time behavior graphs, in order to develop a physical realistic and useful running-in model. A survey of literature revealed eight common forms of coefficient of friction versus sliding time curves. Some of the possible occurrences and causes related to each type of friction curve were intensively discussed

(Blau, 1981). Each type is not uniquely ascribed to a single process or unique combination of processes, but rather must be analyzed in the context of the given tribosystem.

3.2.2 Based on the induced system

Blau (2005) divided the tribological transition of two types, namely induced and non-induced or natural transition. The induced transition is referred to when an operator applies a specified set of the first stage procedures in order to gain the desired surface condition after running-in of certain contacting components. For example, the induced running-in takes place when the new vehicle owner's drive the new car by following the manual book recommendation for the first 100 km.

Non-induced or natural running-in occurs as the system 'ages' without changing the operating contact conditions such as decreasing the load, velocity et cetera. The change of the friction and wear during the sliding contact of a reciprocating piston ring along the cylinder wall is a good illustration of the natural transition. The hydrodynamic or mixed film lubrication regime which is performed during the piston ring reaches its highest sliding velocity at the mid of the stroke. Then, the lubrication regime changes to the boundary film condition when the piston rings reach its lowest velocity at the bottom and top of the stroke. The different regime of lubrication during the piston stroke is realized by the engine designer but the fact that the wear is higher at the bottom or top of the stroke due to the lubrication regime is not intentionally arranged by the designer (Blau, 2005).

3.2.3 Based on the relative motion

Based on the relative motion as explained by Kalker (2000), there are three types of motion, namely rolling, sliding and rolling-sliding contact which generate the different mode in surface topographical change. Considering the surface topographical change during the running in period, there are two dominant mechanisms: plastic deformation and mild wear (Whitehouse, 1980). Shortly after the start of sliding, rolling or rolling-sliding contact between fresh and unworn solid surface, these mechanisms occur.

The rolling contact motion induces the plastic deformation at the higher asperities when the elastic limit is exceeded, as investigated experimentally by Jamari (2006) and Tasan et al. (2007). On the ball on disc system, the rolling contact generates the track groove on the disc rolling path which modifies the rough surface topography after a few cycles on the running-in phase. In this case, the plastic deformation mechanism due to normal loading is a key factor in truncating the higher asperities, decreasing the center line average roughness, R_a, and changing the surface topography (Jamari, 2006).

In the sliding contact, the change of the surface topography is commonly influenced by mild wear, considering several wear mechanisms such as abrasive, adhesive and oxidative. Many models, in predicting the surface topography change on the running-in of sliding contact, proposed with ignoring the plastic deformation (Jeng et al., 2004). Sugimura et al. (1987) pointed that the wear mechanism, i.e. abrasive wear, contributes to the surface topographical change of a Gaussian surface model during running-in of sliding contact. The work continued by Jeng et al. (2004) which introduced the translatory system of a general surface into a Gaussian model. Their works successfully predicted the run-in height distribution of a surface after running-in phase of a sliding contact system.

Running-in of rolling contact with slip, which indicates the rolling-sliding contact, promotes both plastic deformation and wear in modifying the surface topography. Wang et al. (2000)

investigated the change of surface roughness, R_a as a function of sliding/rolling ratio and normal load. The small amount of sliding at the surface increased the wear rate, minimized the time to steady state condition and resulted into a smoother surface than with pure rolling. The combination of the plastic deformation model and wear model in predicting the material removal during the transient running-in of the rolling-sliding contact is proposed by Akbarzadeh and Khonsari (2011). They combined the thermal desorption model, which is the major mechanism of adhesive wear, with the plastic deformation of the asperity in predicting the material removal in macro scale. They measured wear weight, wear depth, surface roughness and coefficient of friction of the two rollers which was rotated for several rolling speeds and slide to roll ratio. The increasing of rolling speed resulted a better protecting film in lubrication regime and reduced the wear weight and wear depth while the increase of the slide to roll ratio increased the sliding distance and generated lower wear rate. The thermal desorption model indicated that increasing of the sliding speed caused the molecules have less time to detach from the surface and therefore the wear volume rate decreased.

4. Running-in of rolling contact model

The models for predicting the surface topography change due to running-in, published in the literature, are mostly related with sliding contact. Started from Stout et al. (1977) and King and his co workers (1978), the topographical changes in running-in phase is predicted by considering the truncating functions of Gaussian surface to obtain the run-in height distribution. Sugimura et al. (1987) continued by proposing a sliding wear model for running-in process which considers the abrasive wear and the effect of wear particles. Due to its limitation of the model for the Gaussian surface, Jeng and co-workers (2004) have developed a model which describes the change of surface topography of general surfaces during running-in.

Other approaches have been applied by researchers for modeling running-in. Lin and Cheng (1989) and Hu et al. (1991) used a dynamic system approach, Shirong and Gouan (1999) used scale-independent fractal parameters, and Zhu et al. (2007) predicted the running-in process by the change of the fractal dimension of frictional signals. Liang et al. (1993) used a numerical approach based on the elastic contact stress distribution of a three-dimensional real rough surface while Liu et al. (2001) used an elastic-perfectly plastic contact model. In running-in of sliding contact, some parameters such as: load, sliding velocity, initial surface roughness, lubricant, and temperature have certain effects. Kumar et al. (2002) explained that with the increase of load, roughness and temperature will increase the running-in wear rate on the sliding contact.

However, based on the literature review, there are less publications discussed the running-in of rolling contact model, especially, dealt with the deterministic contact of rough surface. Most of the running-in models available in literature, is devoted to running-in with respect to wear during sliding motion. These models are designed to predict the change of the macroscopic wear volume or the standard deviation of the surface roughness rather than the change of the surface topography locally on the real engineering surface during the running-in process.

On the next section, an analytical and numerical model are described to propose another point of view in surface topographical change due to running-in of rolling contact. The discussion of the rolling contact motion at running-in phase is focused on the free rolling contact between rigid bodies over a flat rough surface and neglects the tangential force, slip

and friction on the contacted bodies. The point contact is explored in the analytical running-in contact model and experiments while the line contact is observed in numerical model using the finite element analysis.

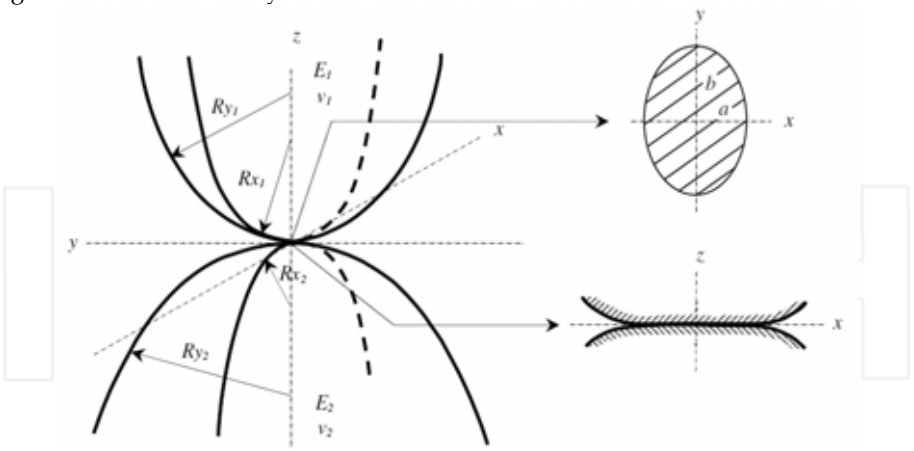

Fig. 4. Geometry of elliptical contact, after Jamari-Schipper (2006)

4.1 Analytical model

The change of surface topography due to plastic deformation of the non-induced running-in of a free rolling contact is presented in this model. On the basis of the elastic-plastic contact elliptical contact model developed by Jamari and Schipper (2006) and the use of the deterministic contact model of rough surfaces which has been explained extensively in Jamari and Schipper (2008), the surface topography changes during running-in of rolling contact is modeled.

Jamari and Schipper (2006) proposed an elastic-plastic contact model that has been validated experimentally and showed good agreement between the model and the experiment tests. In order to predict surface topography after running-in of the rolling contact, they modified the elastic-plastic model of Zhao et al. (2000) and used the elliptical contact situation to model the elastic-plastic contact between two asperities. Figure 4 illustrates the geometrical model of the elliptic contact where a and b express the semi-minor and semi-major of the elliptical contact area. The mean effective radius R_m is defined as:

$$\frac{1}{R_m} = \frac{1}{R_x} + \frac{1}{R_y} = \frac{1}{R_{x1}} + \frac{1}{R_{x2}} + \frac{1}{R_{y1}} + \frac{1}{R_{y2}} \tag{1}$$

R_x and R_y denote the effective radii of curvature in principal x and y direction; subscripts *1* and *2* indicate body *1* and body *2* respectively. The modification of the previous model leads the new equation of the elastic-plastic contact area A_{ep} and the elastic-plastic contact load P_{ep}, which is defined as follows:

$$A_{ep} = 2\pi R_m \omega \frac{\alpha}{\beta} + (2\pi\sqrt{R_x R_y \omega} - 2\pi R_m \omega \frac{\alpha\beta}{\gamma}) \left[3\left(\frac{\omega-\omega 1}{\omega 2-\omega 1}\right)^2 - 2\left(\frac{\omega-\omega 1}{\omega 2-\omega 1}\right)^3 \right] \tag{2}$$

$$P_{ep} = A_{ep}\left[c_h H - H\left(c_h - \frac{2}{3}K_v\right)\frac{\ln\omega_2 - \ln\omega}{\ln\omega_2 - \ln\omega_1}\right] \tag{3}$$

where ω is the interference of an asperity, subscripts *1* and *2* indicate body *1* and body *2* respectively, a and β are the dimensionless semi-axis of the contact ellipse in principal x and y direction respectively, γ is dimensionless interference parameter of elliptical contact, c_h is the hardness factor, H is the hardness of material and K_v is the maximum contact pressure factor related to Poisson's ratio v:

$$K_v = 0.4645 + 0.3141v + 0.1943v^2 \tag{4}$$

The change of the surface topography during running-in is analyzed deterministically and is concentrated on the pure rolling contact situation. Figure 5 shows the proposed model of the repeated contact model performed by Jamari (2006). Here, *h(x,y)* is the initial surface topography. The surface topography will deformed to *h'(x,y)* after running-in for a rolling contact. The elastic-plastic contact model in Eq. 2 and 3 are used to predict the *h'(x,y)*. The calculation steps are iterated for the number/distance of rolling contact.

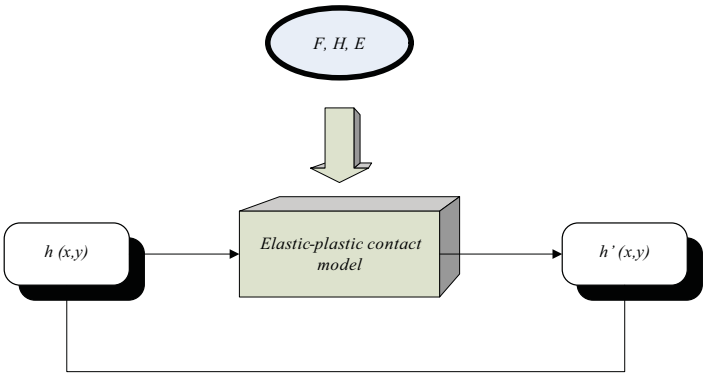

Fig. 5. The model of the surface topography changes due to running-in of a rolling contact proposed by Jamari (2006)

4.2 Finite element analysis of running-in of rolling contact

The next model of running-in of rolling contact is proposed numerically. In order to visualize the topographical change of the rough surface and observe the stress distribution during running-in phase, the two-dimensional finite element analysis (FEA) is conducted. A rigid cylinder was rolled over a rough surface in finite element software by considering the plain strain assumption. The free and frictionless rolling contact was assumed in this model. The cylinder was 4.76 mm in diameter while the asperity height on rough surface, Z_{as}, was 0.96 mm, the spherical tip on the summit of asperity, R_a, was 0.76 mm and the pitch of the rough surface, P was 1.5 mm. The dimensions of the rough surface control its wave length and amplitude. The model, simulation steps and validation, described respectively in this section, have been used in the previous FEA of rolling contact simulation (Ismail et al., 2010).

4.2.1 Material model and simulation steps

The rough surface was modeled as aluminum and was considered as elastic- plastic material with strain hardening behavior where the behavior of the stress versus strain curve was obtained from the tensile test conducted by Bhowmik (2007). The curve described the strain hardening effect of the elastic-plastic material model and had been verified with his experiments and finite element simulations. For the rough surface, the elastic modulus (E), yield stress (S_y), and Poisson's ratio (υ) were 70 GPa, 270 MPa, and 0.32, respectively whereas the cylinder was assumed to be a rigid body so that there is no deformation occured during rolling contact.

The four nodes element with plain strain model was specified on the rough surface with the refine mesh was applied on the top of the rough surface. As depicted in Fig. 6, the refinement was also set on one of the asperity (at the center position) from the asperity summit to the bulk material for better investigation on the contact stress and residual stress.

The simulation steps in FEA, as shown in Fig. 6, were conducted as follows: (a) the normal static contact was applied on the cylinder over the rough surface for an interference, ω; (b) by maintaining the vertical interference, the cylinder rolled over to the right direction incrementally until reached the end of the rough surface and the cylinder was moved up for unloading; (c) the rolling contact of the cylinder over the rough surface was repeated for three times in order to observe the transition of the running-in phase.

In order to compare the topographical change, contact stress and residual stress of the rolling contact, another simulation was carried out by conducting the repeated static contact of the rigid cylinder to the rough surface. The three steps on the repeated static contact were conducted as follows: (a) the normal static contact was applied on the cylinder over the rough surface with certain interference, ω; (b) unloading the contact load by moving the cylinder up to the origin position; and (c) repeating this loading and unloading contact for three cycles. The same interferences and the same model were used in the repeated rolling contact and repeated static contact.

4.2.2 FEM model verification

The critical interference, ω_c, and the critical contact width b_c proposed by Green (2005) for determining the yielding limit between the elastic and the elastic-plastic deformation of line contact were used to verify the model. These equations, derived by using the distortion energy yield criterion of maximum von Mises stress, are defined as:

$$\omega_c = R\left(\frac{CS_y}{E}\right)^2\left[2\ln\left(\frac{2E'}{CS_y}\right)-1\right] \tag{5}$$

$$b_c = \frac{2R(CS_y)}{E'} \tag{6}$$

where $C = 1.164 + 2.975\upsilon - 2.906\,\upsilon^2$ and E' is the equivalent elastic modulus. The analytical equations were compared with the results of the finite element simulation of the present model in predicting the yielding of the model.

Based on Eq (5) and (6), the critical interference and the critical contact width of the static contact between a rigid cyclinder versus a single asperity are 9.53×10^{-5} mm and 2.88×10^{-3} mm, respectively. A single asperity is employed as a representation of the rough surface.

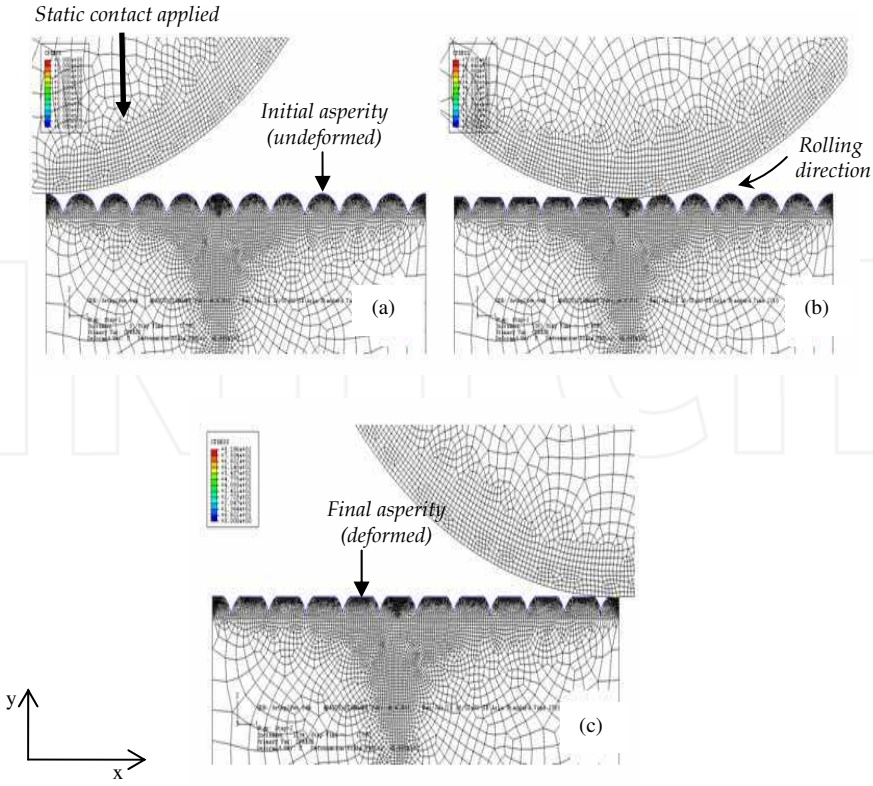

Fig. 6. The rolling contact simulation: (a) start from the static contact, (b) followed by rolling contact with maintaining the contact load, and (c) the roller reaches the end of the rough surface and is unloaded

When the calculated ω_c is applied on the present model of the finite element simulation, the measured contact width in FEA is 3 x 10^{-3} mm. The result implies the rational agreement between the analytical and numerical results where the deviation is 4.16 %. Then the von Mises yield stress criterion in the FEA was used to check the maximum stress. The obtained maximum yield stress indicates that the material starts to yield and the deformation is categorized in elastic-plastic regime. By comparing the von Mises stress of the obtained value in FEA (249.7 MPa) and the yield stress of the material model 270 MPa, a deviation of 7.52 % is found. The comparison of the analytical calculation and numerical simulation is listed in Table 1.

The previous critical interference and contact width are relatively small compared to the analytical calculation of the contact between the rigid cylinder with a flat surface. The analytical result of the critical interference and contact width in this case, where ω_c and b_c are 1.98 x 10^{-3} mm and 5.99 x 10^{-2} mm, respectively, are twenty times higher compared to the previous calculation. The accuracy of the analytical calculation of this model, compared to the results in FEA, increase significantly where the deviation of the contact width and the maximum von Mises stress are 2.93% and 0.13%, respectively. Table 1 shows the comparison

between the prediction of the analytical model (Green, 2005) and the numerical simulation of single static contact occupying the present model. The table exhibits the transition of the elastic to elastic-plastic deformation with respect to the ω_c, the b_c and the maximum von Mises stress.

Contacting Bodies	ω_c analytic (mm)	b_c analytic (mm)	b_c numeric (mm)	Diff. of b_c (%)	Max stress (vM) numeric (MPa)	Diff. of max stress (%)
Cylinder vs singe asperity	9.53×10^{-5}	2.88×10^{-3}	3×10^{-3}	4.2	249.7	7.5
Cylinder vs flat surface	1.98×10^{-3}	5.99×10^{-2}	5.98×10^{-2}	0.1	262.1	2.9

Table 1. Comparison between the analytical model and numerical simulation for determining the transition of the elastic to elastic-plastic deformation for the static contact of the present FE model

The conclusion of the model verification is the present finite element simulation has a good agreement with the previous analytical model in predicting the critical interference, critical contact width and the maximum von Mises stress. However, the lower deviation, which is found in the contact between cylinder versus flat, argues that the Green's model has an opportunity to be derived by considering the contact between cylinders with the high ratio of the diameters such as the contact between cylinder and one asperity in this case. The modification of the new model is planned as the future work such that the prediction of the elastic-plastic deformation of two-dimensional rough surface can be done analytically.

4.2.3 Topographical change due to repeated rolling contact

In order to demonstrate the effect of the rolling contact to the asperity and the bulk material, the interferences in this simulation are set larger than the critical interference. Two interferences, $\omega_1 = 2 \times 10^{-2}$ mm and $\omega_2 = 4 \times 10^{-2}$ mm, are employed in this model to analyze the plastic deformation and the material transfer as well as the contact stress and the residual stress during and after the rolling contact. Respectively, these applied interferences are nearly 10 times and 20 times higher than critical interference of the contact model between the cylinder and flat surface.

Figure 6 shows the topographical evolution from the initial undeformed, contacted and the final deformed asperities due to plastic deformation of rolling contact. The asperity height on the rough surface is truncated and some materials are displaced after the rigid cylinder rolls over the rough surface. The observation is focused on a single asperity as a representative of the rough surface. Surface topographical changes of an asperity after several rolling contacts are presented in Fig. 7.

The change of the asperity height due to rolling contact can be seen on Fig. 7 (a) for ω_1 and Fig. 7 (b) for ω_2. The dashed and solid lines show the situation before and after the rolling contact deformation, respectively. The deformation was captured after the unloading of each cycle of the rolling contact. The figures exhibit that the first cycle causes the highest deformation and it is followed by only slight deformation at the second cycle. There is no significance difference on the asperity height after the second cycle which implies that, in this case, the steady state deformation is reached. The transition of the running-in of rolling contact occurs at the cycle 2.

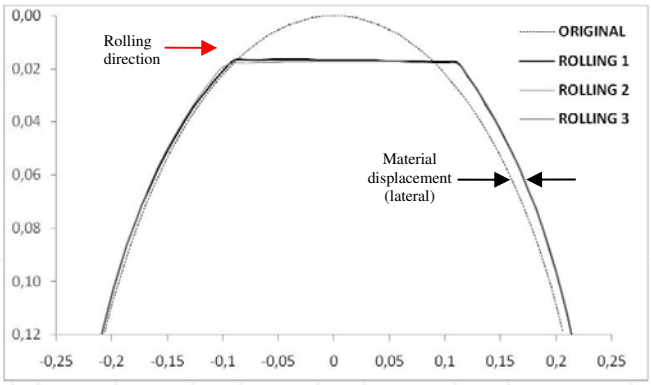

(a)

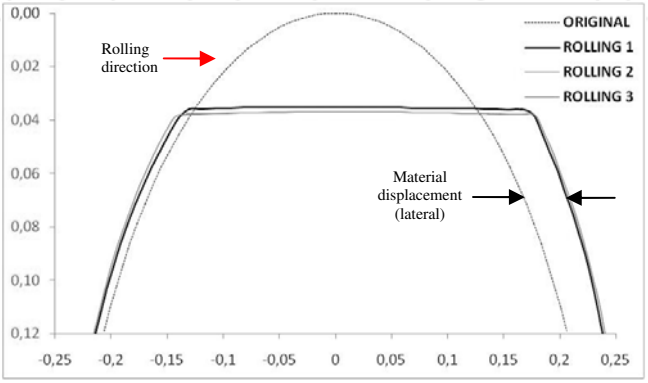

(b)

Fig. 7. Surface topographical change of a single asperity due to repeated rolling contact for: (a) $\omega_1 = 2 \times 10^{-2}$ mm and (b) $\omega_2 = 4 \times 10^{-2}$ mm

On their FEA of rolling cylinder of a deformable flat, Bijak-Zochowski and Marek (2007) also found that the steady state deformation was usually attained within the first two cycles for repeated rolling contact. The deformation for the next rolling has a small difference. The next discussion of the experimental running-in of rolling contacts, Jamari (2006) also reported that the censoring higher asperity of the rough surface is initially high on the first ten rolling cycle while Tasan et al. (2007) obviously resumed that the first rolling contact has a highest deformation and it is followed by the slight deformation for the next cycles.

The flattening of the asperities on the first rolling cycle means that the conformity of the contact increases during plastic deformation. With the increase of the contact conformity, the contact area gets wider, and the contact stress become more homogeneously distribute. The increasing conformity and contact area induce the stability of the plastic deformation on the asperities.

Considering the material displacement of the finite element simulation on Fig 7 (a) and (b), the material on the summit of the asperity is displaced laterally on the same direction of the rolling contact. The discussion of the material displacement is explored on the next section.

4.2.4 Stresses of rolling contact

The observation of the contact stress and the residual stress during and after the first cycle of repeated rolling contact for ω_2 is depicted on Fig. 8 (a) and (b), respectively. These figures are captured during and after the first rolling contact. Figure 8 (a) depicts the situation when the rigid cylinder is located at the centre of the contacted asperity, which is marked with the wide area of von Mises stress distribution while Fig. 8 (b) shows the residual stress after the first rolling contact is finished and unloaded.

The discussion of rolling contact stress is focused on the contacted asperity where the plastic deformation is easily noticed on the summit of the asperity and the maximum von Mises stress area reaches the surface. When the applied interference below its critical point and the deformation still behaves elastically, the highest von Mises stress area is located on the sub surface, few distances below the surface. The highest von Mises stress area moves to attain the surface as the applied interference is higher than the critical interference. This plastic deformation phenomenon was also discussed Jackson and Green (2005) which modelled the elastic-plastic static contact between the hemisphere and the rigid flat. Fig 8 (a) also depicts the plastic flow when the cylinder rolls over an asperity. The plasticity is formed on the right side of the asperity and produces a lateral material displacement as the same direction of the rolling motion.

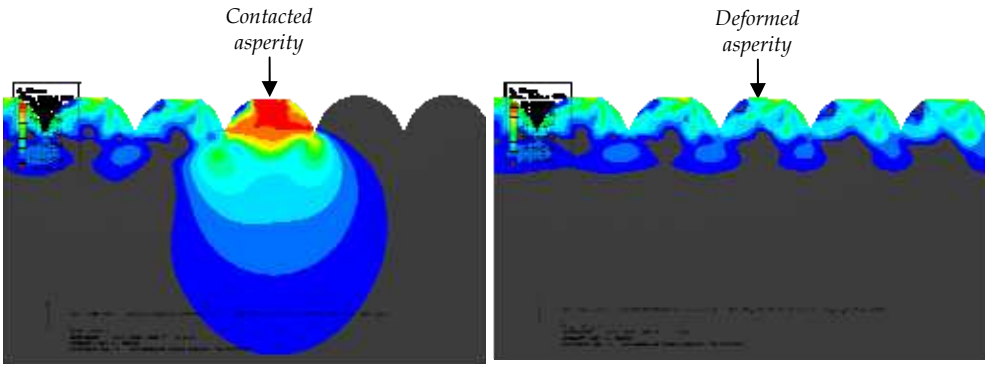

Fig. 8. The von Mises stress analysis for $\omega_2 = 4 \times 10^{-2}$ mm: (a) during the first rolling contact and (b) residual stress after the first rolling contact.

The von Mises stress of the contact stress and the residual stress are plotted as a function of the depth of the rough surface for the three repeated rolling contact, as seen in Figure 9 (a) and (b), respectively. In Fig. 9 (a), the behaviour of the stress distribution on the surface of the three repeated rolling contact only has a slight difference but at the subsurface of the asperity until the bulk material, the second and third rolling contact has a lower von Mises stress. The stress decreases after the first rolling contact and it is predicted that the material become harder due to strain hardening behavior. Kadin, et al. (2006) which studied the multiple loading-unloading of a spherical contact also reported the stability of plasticity distribution on the second loading-unloading contact. The linear strain hardening behavior was pointed as the causes of this phenomenon.

After the rolling cylinder is unloaded for each rolling contact, the stress distributions are captured again for analyzing the residual stress. Figure 8 (b) shows that the highest residual stress is found on the flattened asperity summit. Based on Fig. 9 (b) which depicts the residual stress as a funtion of the depth by using the von Mises criteria, the curves of three repeated rolling contact is nearly coincided after depth reaches 0.15 mm. The maximum of the residual stress, located on the asperity summit, from the first until the third rolling contact is increase from 179.7 MPa, 220.8 MPa and 248.8 MPa, respectively. The increase of the residual stress is a consequence of the strain hardening behavior on plastic the deformation. The material strain hardening on the summit of asperity has a protective effect in reducing further plastic deformation and induces a stability of the deformation after the first rolling contact.

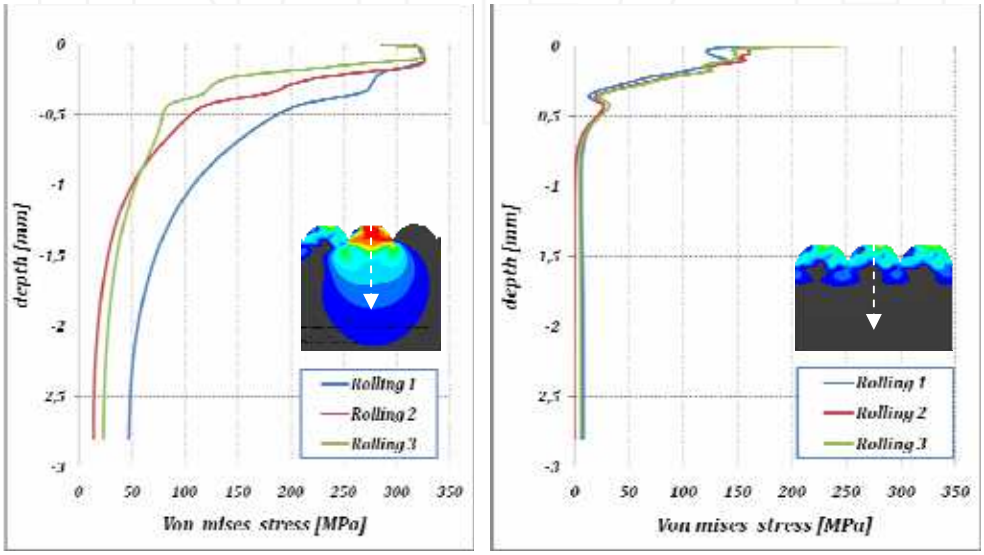

Fig. 9. von Mises Stress analysis (a) during rolling contact and (b) residual stress after the rolling contact finish.

The strength and expected life of mechanical components can be influenced by residual stress due to its effect on contact fatigue and wear (Bijak-Zochowski and Marek, 2007). Nelias and his co-workers (2006), assumed that the volume of material will detach from the surface after very few cycles. The detachment of the material occurs when the equivalent plastic strain found after unloading, located at the surface, exceeds a threshold value. Nelias et al. (2006) determined that the threshold value of the equivalent plastic strain is 0.2 %. In this present model, the maximum residual stress is found on the summit of the asperities which able to lead the detachments. The investigation are planed in the future for analizing the wear and the equiavalent plastic strain by combining the FEA model and Nelias et al. model (2006).

4.2.5 Comparison with the repeated static contact

Jamari (2006) reported three methods in repeated contact on the rough surface for observing the topographical change: (a) repeated static contact; (b) repeated moving contact; and (c)

repeated rolling contact. The proposed elastic-plastic contact model of Jamari and Schipper (2006) could predict the three types of the repeated contact quite well. In the case of free or pure rolling contact, it does not contain a tangential force. Therefore, it is reasonable that this type of motion can be modeled by multiple-indentation of one body to another body without changing the indentation position.

A comparison between the repeated rolling contact and the repeated static contact is discussed to show the difference of the topographical change for the both mechanisms. The topographical change of a single asperity due to repeated static contact is depicted in Fig. 10. It shows the symmetrical material displacement on the both side of the asperity, whereas in the repeated rolling contact, the asymmetrical material displacement is found with the majority of the material is displaced at the same direction of the rolling, as seen in Fig 7 (a) and Fig 7 (b). The deformed asperity on the repeated static contact shows that the centre of the asperity summit has larger deformation than its edge whereas on the repeated rolling contact the deformation is almost flat from the edge and centre of the asperity.

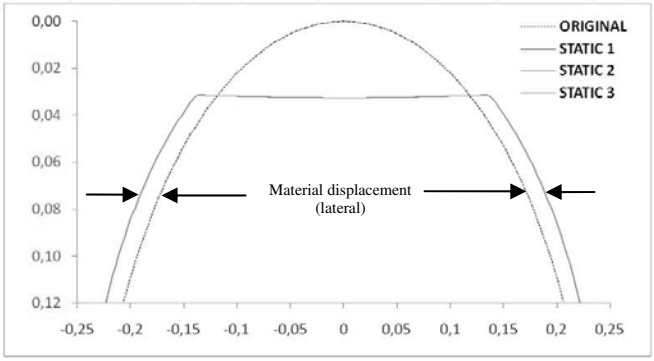

Fig. 10. The surface topographical change due to repeated static contact for a single asperity for $\omega_2 = 4 \times 10^{-2}$ mm

The von Mises stress distribution of the repeated static contact for ω_2 is shown in Fig. 11 (a) for the stresses during first loading and in Fig. 11 (b) for residual stress after the first unloading. It can be seen on the Fig. 11 (a) that the cylinder is in contact with three asperities and the highest contact stress takes place on the middle asperity. The centre of the middle asperity deformation due to repeated static contact is observed in Fig. 10. The concave shape

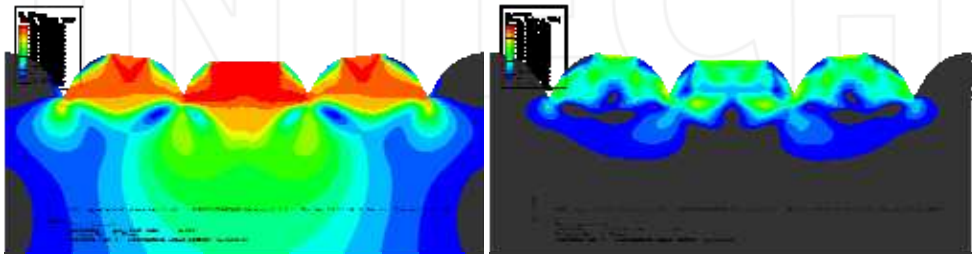

Fig. 11. The von Mises Stress analysis for $\omega_2 = 4 \times 10^{-2}$ mm: (a) during first static contact and (b) residual stress after the first static contact finish.

on the asperity surface is formed as the consequences of the highest contacted stress on the centre of the asperity. In Fig. 11 (b) the residual stress is found on the summit of the asperity and on the some area in bulk material, especially on the sharp valley of the rough surface. On the centre of the middle asperity, both of the contacted stress and residual stress on the repeated static contact perform symmetrical stress distribution.

5. Running-in of rolling contact experiments

Two running-in of rolling contact experiments of Jamari (2006) and Tasan et al. (2007) are presented in this section. There are two goals in discussing the experiments of running-in of rolling contact. First, the experiments are used to validate the running in model of Jamari (2006) which has been explored on the previous section. Second, the experiments are employed for investigating the change of the surface topography due to running-in of rolling contact at the lateral and longitudinal of rough surface direction.

The running-in of rolling contact experiments are conducted on the measurement setup where the details of the arrangement of the setup are presented in Fig. 12(a). The spherical indenter (ball specimen) is held by the clamping unit. The loading arm and the rotating table are positioned on the X-Y table such that the spherical indenter is located on one side of the disk, whilst the interference microscope is positioned on the other side of the disk and stands separately from the X-Y table. Figure 12(b) depicts the detail of ball holder and the position of the ball specimen.

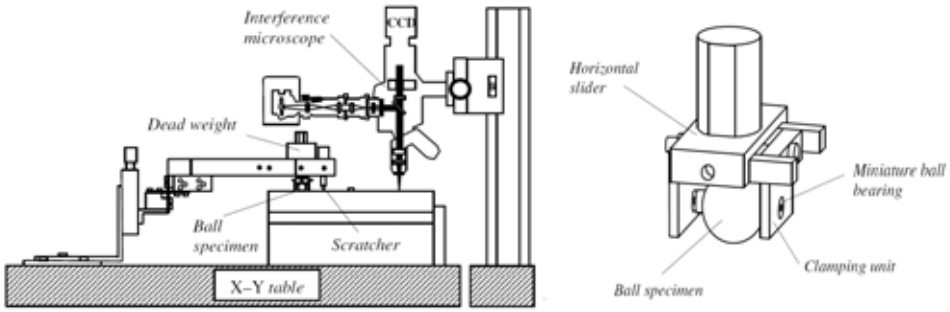

(a) (b)

Fig. 12. (a) The main view of semi on-line measurement of running-in rolling contact and (b) the rolling ball specimen and the holder (Jamari, 2006)

Silicon carbide ceramic balls SiC (H = 28 GPa, E = 430 GPa and v = 0.17) with a diameter of 6.35 mm were used as hard spherical indenters. The center line average roughness Ra of the ceramic ball of 0.01 mm was chosen to comply with the assumption of a perfectly smooth surface. Elastic-perfectly plastic aluminium (H = 0.24 GPa, E = 75.2 GPa and v = 0.34) and mild-steel (H = 3.55 GPa, E = 210 GPa and v = 0.3) were used for the rough flat surface specimens. The center line average roughness of the flat specimens varied from 0.7 to 2 mm.

Results of the rolling contact experiment, along with the model prediction for the aluminium and mild-steel surfaces are presented in Fig. 13 (a) and (b), repsectively. It can be seen that the change of the surface deformation for each number of rolling contact reaches

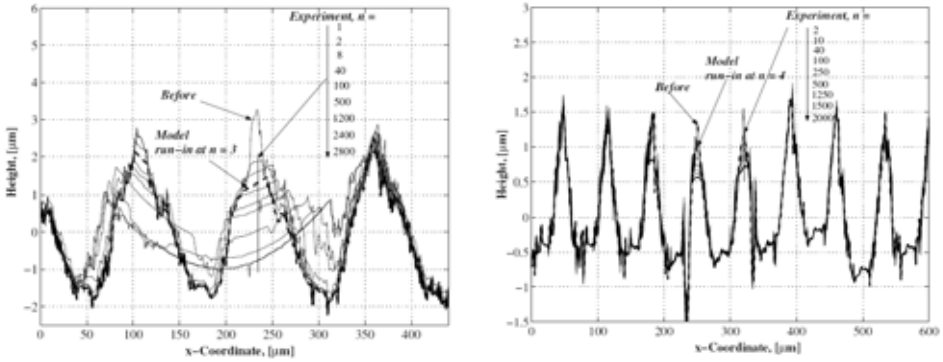

(a) (b)

Fig. 13. Profile of the matching and stitching result across the direction of rolling of (a) aluminium surface at y = 160 mm and (b) mild-steel surface at y = 158 mm (Jamari, 2006)

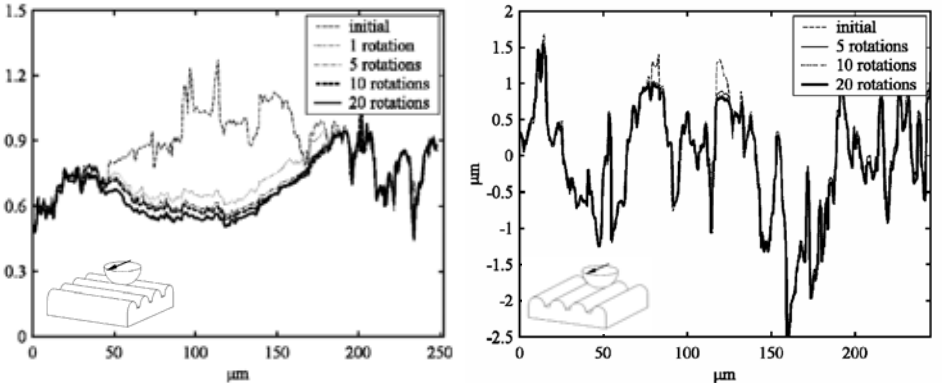

(a) (b)

Fig. 14. Profiles across the direction of rolling for (a) lateral and (b) longitudinal roughness as the function of the number of rolling cycles (Tasan, et al, 2007)

its highest gap on the first 10 cycles. There is only slight difference on the surface topographical change for each number of rolling contact after the first 10 cycles. Hsu et al. (2005) concluded that as the contact progresses to a nearly steady-state operation, the surface roughness of the tribocontacts becomes less variable. The model predicts the surface topographical change at cycle n = 3 for the aluminium surface and at cycle n = 4 for the mild-steel surface. The proposed model performs a rational agreement with the experiments for the mentioned number of rolling contact. However, on the set-up of the rolling contact experiment, the slight presence of slip is can not be avoided where its appearance can switch the pure rolling contact motion to the rolling contact with slip or rolling-sliding contact.

Compares to the Jamari's experiments, the investigations of Tasan et al (2007) on the topographical change after rolling contact between an SiC ball in contact with a rough mild steel disk (DIN 100MnCrW4) are presented. A semi on-line measurement setup was utilized to perform rolling contact experiments where the detail description can be found in (Tasan, 2005). Figure 14 depicts the topographical change of the surface on (a) the lateral direction and (b) the longitudinal direction due to running-in of rolling contact. On the lateral and longitudinal direction of this case, it is found that the rough surface deformed plastically on the contacted area at the first five cycle, where the largest deformation occurred on the first cycle, and then the deformation decreases and reaches its steady state. The experiments also exhibit the running-in phase of the rolling contact and followed by the steady state phase afterward.

In finite element simulation in Fig. 7(a), it also performs the lateral material displacement due to rolling contact experiments. The lateral displacement can be happen when there is some space for the material to be removed plastically. In repeated rolling contact, the displacement indicates that the plastic deformation is more dominant in topographical change on the asperity level rather than material removal due to wear mechanisms.

6. Concluding remarks

The studies of topographical change due to running-in of rolling contact are presented in this book chapter analytically, experimentally and numerically. A running-in model of rolling contact by considering the deterministic contact of the engineering surface has been proposed. The proposed model of running-in of rolling contact performs a good agreement with the experiments. Finite element simulations of two-dimensional rolling contact model contribute in illustrating the truncation on the asperity summit, the contact stress and the residual stress due to plastic deformation. The comparison of the repeated static contact and the repeated rolling contact leads un-similarity in material transfer direction and asperity deformation.

As the critical effect of the surface topography on the running-in stage for prolonging the lifespan of the contacted mechanical components, this investigation can contribute in predicting the initial, the change, and the final of the surface topography for a success running-in stage. Running-in plays an important role in plastic deformation, friction and wear of tribology systems during the steady-state period. Ignoring the running-in aspects means overlooking the important clues to the evolution of conjoint processes which leads to the final long-term steady-state friction and wear behavior.

7. References

Akbarzadeh, S. & Khonsari, M.M. (2011). Experimental and Theoretical Investigation of Running-in, *Tribology International*, Vol. 44, (February 2011), pp. 92-100, ISSN 0043-1648

Bhowmik, K. (2009). *Experimental and Finite Element Study of Elastic-Plastic Indentation of Rough Surfaces*, Master Thesis, Indian Institute of Science, Bangalore, India

Bijak-Zochowski, M. & Marek, P. (1997). Residual Stress in Some Elasto-Plastic Problems of Rolling Contact with Friction, *International Journal of Mechanic Science,* Vol. 39. No. 1, (January 1997), pp. 15-32, ISSN 0020-7403

Blau, P.J. (1981). Interpretations of the Friction and Wear Break-in Behaviour of Metal in Sliding Contact, *Wear,* Vol. 71, (September 1981), pp. 29 – 43, ISSN 0043-1648

Blau, P.J. (1989). *Friction and Wear Transitions of Materials: Break-in, Run-in, Wear-in*, Noyes Publications, ISBN 0-815-511965, Park Ridge, NJ, USA

Blau, P.J. (2005). On the Nature of Running-in, *Tribology International,* Vol. 38, (August 2005), pp. 1007 – 1012, ISSN 0043-1648

Halling, J. (1976) *Introduction to Tribology*, Wykeham Publication Ltd., ISBN 0387911286, London, UK

Green, I. (2005). Poisson Ratio Effects and Critical Values in Spherical and Cylindrical Hertzian Contacts, *International Journal of Applied Mechanics*, Vol. 10, No. 3, pp. 451-462

Hu, Y.Z.; Li, N. & Tonder, K. (1991). A Dynamic System Model for Lubricated Sliding Wear and Running-in, *ASME Journal of Tribology* , Vol. 113, No. 3, (July 1991), pp. 499 – 505, ISSN 0742-4787

Hsu, S.M.; Munro, R.G.; Shen, M.C. & Gate, R.S. (2005). Boundary Lubricated Wear, In: *Wear-Materials, Mechanisms & Practice,* G.W. Stachowiak (Ed.), 37-69, John Wiley & Sons Inc., ISBN 978-0-470-01628-2, London, UK

Ismail, R.; Tauviqirrahman, M.; Jamari & D.J. Schipper. (2010). Elastic-Plastic Deformation of a Rough Surface Due To Repeated Rolling Contact, *Proceeding of International Conference on Physics and Its Applications*, Solo, Indonesia, pp. 49-52

Jackson R.L. & Green I. (2005). A Finite Element Study of Elasto-plastic Hemispherical Contact. *ASME Journal of Tribology,* Vol. 127, (April, 2005), pp. 343–54, ISSN 0742-4787

Jamari, J. (2006). *Running-in of Rolling Contacts*. PhD Thesis, University of Twente, Zutphen, ISBN: 90-365-2314-1, Enschede, The Netherlands

Jamari, J. & Schipper, D.J. (2006). An Elastic-Plastic Contact Model of Ellipsoid Bodies, *Tribology Letters*, Vol. 21, No. 3, (March, 2006), pp. 262-271, ISSN 1573-2711

Jamari, J. & Schipper, D.J. (2008). Deterministic Repeated Contact of Rough Surfaces, *Wear,* Vol. 264, (February 2008), pp. 349–358, ISSN 0043-1648

Jeng, Y.R. (1996). Impact of Plateaued Surfaces on Tribological Performance, *Tribology Transaction* Vol. 39, pp. 354 – 361, ISSN 1547-397X

Jeng, Y.R.; Lin, Z.W. & Shyu, S.H. (2004). Changes of Surface Topography during Running-in Process, *ASME Journal of Tribology,* Vol. 126, No. 3, pp. 620 – 625, ISSN 0742-4787

Johnson, K.L. (1985). *Contact Mechanics*, Cambridge University Press, ISBN 0-521-347963, Cambridge, England

Kadin, Y.; Kligerman, Y. & Etsion, I. (2006). Multiple Loading–Unloading of an Elastic–Plastic Spherical Contact, *International Journal of Solid and Structure,* Vol. 43, (November 2006), pp. 7119-7127, ISSN 0020-7683

Kalker, J.J. (2000). Linear Elasticity in Rolling Contact, In: *Rolling Contact Phenomena*, B. Jacobson & J.J. Kalker (Ed.), 1-16, Springer-Verlag Wien ISBN 3-211-83332-3, New York, USA

Kehrwald, B. (1998). *Einlauf Tribologischer Systeme*, Ph.D. Thesis, University of Karlsruhe, in German

King, T.G.; Watson, W. & Stout, K.J. (1978). Modelling the Micro-geometry of Lubricated Wear, *Proc. 4th Leeds-Lyon Symposium*, pp. 333 – 343, MEP, London, UK

Kraghelsky, V.; Dobychun, M.N. & Kombalov, V.S. (1982). *Friction and Wear Calculation Methods*, Pergamon Press, ISBN 0080254616, Oxford, UK

Kumar, R.; Prakash, B. & Sethuramiah, A. (2002). A Systematic Methodology to Characterize the Running-in and Steady-state Processes, *Wear,* Vol. 252, (March 2002), pp. 445 – 453, ISSN 0043-1648

Liang, X.; Kaiyuan, J.; Yongqing, J. & Darong, C. (1993). Variations in Contact Stress Distribution of Real Rough Surfaces During Running-in, *ASME Journal of Tribology,* Vol. 115, Vol. 4, (October 1993), pp. 602 – 606, ISSN 0742-4787

Lin, J.Y. & Cheng, H.S. (1989). An Analytical Model for Dynamic Wear, *ASME Journal of Tribology,* Vol. 111, Vol. 3, (July 1989), pp. 468 – 474, ISSN 0742-4787

Liu, Z.; Neville, A. & Reuben, R.L. (2001). Analyzing Elastic-Plastic Real Rough Surface Contact in Running-in, *Tribology Transactions,* Vol. 44, pp. 428 – 436, ISSN 1547-397X

Shirong, G. & Gouan, C. (1999). Fractal Prediction Models of Sliding Wear during the Running-in Process, *Wear,* Vol. 231, (July 1999), pp. 249 – 255, ISSN 0043-1648

Stout, K.J.; Whitehouse, D.J. & King, T.G. (1977). Analytical Techniques in Surface Topography and Their Application to a Running-In Experiment, *Wear,* Vol. 43, (May 1977), pp. 99 – 115, ISSN 0043-1648

Summer-Smith, J.D. (1994). *An Introductory Guide to Industrial Tribology*, Mechanical Engineering Publications Limited, ISBN 0-85298-896-6 London, UK

Summer-Smith, J.D. (1997). *A Tribology Casebook*, Mechanical Engineering Publications Limited, ISBN 0-85298-896-6 London, UK

Sugimura, J.; Kimura, Y. & Amino, K. (1987). Analysis of the topography changes due to wear–Geometry of the running-in process, *JSLE* , Vol. 31, No.11, pp. 813 – 820

Tasan, Y.C., (2005). *Measurement of Deformation in Rolling and Sliding Contacts*, PhD Thesis, University of Twente, Print Partners Ipskamp B.V., ISBN 90-365-2193-9, Enschede, The Netherlands

Tasan, Y.C.; de Rooij, M.B. & Schipper, D.J. (2007). Changes in the Micro-geometry of a Rolling Contact, *Tribology International*, Vol. 40, (April, 2007), pp. 672–679, ISSN 0043-1648

Wang, W.; Wong, P.L. & Zhang, Z. (2000). Experimental Study of the Real Time in Surface Roughness during Running-in for PEHL Contacts, *Wear,* Vol. 244, (August 2000), pp. 140 – 146, ISSN 0043-1648

Whitehouse, D.J., 1980, "The Effect of Surface Topography on Wear," in *Fundamentals of Tribology,* edited by Suh and Saka, The MIT Press, ISBN 978-0262191838, pp. 17-52, Massachusetts, USA

Zhao, Y.; Maietta, D.M. & Chang, L. (2000). An Asperity Microcontact Model Incorporating the Transition from Elastic Deformation to Fully Plastic Flow, *ASME Journal of Tribology,* Vol. 122, (January 2000), pp. 86 – 93, ISSN 0742-4787

Zhu, H.; Ge, S.; Cao, X. & Tang W. (2007). The change of fractal dimension of frictional signals in the running-in wear process, *Wear*, Vol. 263, (September, 2007), pp. 1502-1507, ISSN 0043-1648

INTECH

INTECH

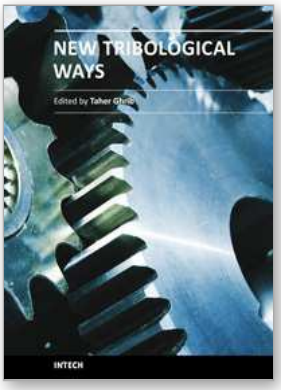

New Tribological Ways

Edited by Dr. Taher Ghrib

ISBN 978-953-307-206-7
Hard cover, 498 pages
Publisher InTech
Published online 26, April, 2011
Published in print edition April, 2011

This book aims to recapitulate old information's available and brings new information's that are with the fashion research on an atomic and nanometric scale in various fields by introducing several mathematical models to measure some parameters characterizing metals like the hydrodynamic elasticity coefficient, hardness, lubricant viscosity, viscosity coefficient, tensile strength .... It uses new measurement techniques very developed and nondestructive. Its principal distinctions of the other books, that it brings practical manners to model and to optimize the cutting process using various parameters and different techniques, namely, using water of high-velocity stream, tool with different form and radius, the cutting temperature effect, that can be measured with sufficient accuracy not only at a research lab and also with a theoretical forecast. This book aspire to minimize and eliminate the losses resulting from surfaces friction and wear which leads to a greater machining efficiency and to a better execution, fewer breakdowns and a significant saving. A great part is devoted to lubrication, of which the goal is to find the famous techniques using solid and liquid lubricant films applied for giving super low friction coefficients and improving the lubricant properties on surfaces.

How to reference

In order to correctly reference this scholarly work, feel free to copy and paste the following:

R. Ismail, M. Tauviqirrahman, Jamari and D.J. Schipper (2011). Topographical Change of Engineering Surface due to Running-in of Rolling Contacts, New Tribological Ways, Dr. Taher Ghrib (Ed.), ISBN: 978-953-307-206-7, InTech, Available from: http://www.intechopen.com/books/new-tribological-ways/topographical-change-of-engineering-surface-due-to-running-in-of-rolling-contacts

INTECH
open science | open minds

InTech Europe
University Campus STeP Ri
Slavka Krautzeka 83/A
51000 Rijeka, Croatia
Phone: +385 (51) 770 447
Fax: +385 (51) 686 166
www.intechopen.com

InTech China
Unit 405, Office Block, Hotel Equatorial Shanghai
No.65, Yan An Road (West), Shanghai, 200040, China
中国上海市延安西路65号上海国际贵都大饭店办公楼405单元
Phone: +86-21-62489820
Fax: +86-21-62489821